Supporting Information

Text S1

NaOH, HCl, H_2SO_4, KPS, Ag_2SO_4, $HgSO_4$, $K_2Cr_2O_7$, $(NH_4)_2Fe(SO_4)_2 \cdot 6H_2O$ $C_{12}H_8N_2 \cdot H_2O$, $FeSO_4 \cdot 7H_2O$, $AlCl_3 \cdot 6H_2O$, Na_2CO_3 were purchased from Shanghai Titan Scientific Co., China. PAM was obtained from Aladdin Industrial Co., Ltd. Methacryloyoxyethyl trimethyl ammonium chloride (DMC, 75 wt.%) was obtained from Macklin Co., Ltd.

The papermaking sludge was obtained from a paper mill in Linyi, Shandong province. The lignin content of the papermaking sludge above was 38.2±4.6. Total analysis of heavy metals in papermaking sludge is shown in Table S1.

Table S1 Total analysis of heavy metals in papermaking sludge.

Number	Element	Content (mg/Kg)	Number	Element	Content (mg/Kg)
1	Li	4.35	31	In	0.09
2	Be	0.18	32	Sn	3.40
3	Na	7675.86	33	Sb	29.05
4	Mg	6976.71	34	Cs	0.59
5	Al	92637.44	35	Ba	238.75
6	K	2150.51	36	La	6.65
7	Ca	14030.27	37	Ce	16.03
8	Sc	26.10	38	Pr	1.44
9	Ti	548.52	39	Nd	10.90
10	V	78.37	40	Sm	0.97
11	Cr	433.01	41	Eu	0.40

12	Mn	1762.90	42	Gd	1.01
13	Fe	18691.83	43	Tb	0.18
14	Co	2.08	44	Dy	0.98
15	Ni	97.37	45	Ho	0.17
16	Cu	11.20	46	Er	0.53
17	Zn	96.97	47	Tm	0.06
18	Ga	41.44	48	Yb	0.36
19	Ge	0.28	49	Lu	0.08
20	Rb	12.81	50	Hf	2.42
21	Sr	146.27	51	Ta	0.08
22	Y	4.50	52	W	1.39
23	Zr	93.97	53	Au	0.30
24	Nb	1.53	54	Hg	0.20
25	Mo	5.65	55	Tl	0.34
26	Ru	0.08	56	Pb	32.32
27	Rh	0.00	57	Bi	0.28
28	Pd	1.14	58	Th	5.40
29	Ag	0.44	59	U	1.24
30	Cd	1.07			

Text S2

Preparation procedures of PSBF

i) Five grams of dried papermaking sludge were dissolved with 180-200 ml of deionized water. Next, the mixture was adjusted to pH 12.0-12.5 by 0.1 M HCL and 0.1 M NaOH solutions.

ii) The supernatant was collected and adjusted to pH 7.8-8.0, and then it was transferred into a three-neck flask.

iii) KPS (0.05 g) and EDTA-2Na (0.05 g) were added into the mixture and stirred for 20 min.

iv) Finally, 30 mL of DMC was dropwise added into the reactor and stirred for 4 h. The reaction was carried out at 70 □ in a water bath with continuous nitrogen protection. The target product was dissolved in ethanol, and then the residual DMC monomers precipitated in acetone. After that, the product was dried at 50 □ in a vacuum oven. The dried PSBF powders were prepared to 10.0 g/L and 1.0 g/L solutions with a certain amount of deionized water in this work.

Text S3

Determination of the COD-Dichromate method

i) Accurate 5 mL of coagulation effluent was collected and diluted 10 times with deionized water.

ii) 10 mL of diluted water samples was added into the Erlenmeyer flask, and then some boiling beads, 2 mL $HgSO_4$ solution and 5 mL $K_2Cr_2O_7$ solution were sequentially added into the flask.

iii) Then, the Erlenmeyer flask was equipped with a reflux, and 15 mL of concentrated H_2SO_4 was slowly added into the flask via the top of the condenser.

iv) The mixture was heated at 198 □ and kept boiling for 2 h.

v) About 45 mL of deionized water was added into the flask via the top of the condenser after the

mixture has cooled to the room temperature.

vi) The waster samples were titrated by the 0.05 mol/L of $(NH_4)_2Fe(SO_4)_2 \cdot 6H_2O$ solution, and the ferroin indicator solution was used as indicator.

vii) The blank test was conducted based on the procedures above, but 10 ml of water sample was replaced by 10 mL of deionized water.

The COD_{Cr} of the effluent was calculated by the following equation (Eq):

$$COD_{Cr}(\frac{mg}{L}) = \frac{C \times (V_0 - V_1) \times 8000}{V_2} \times f \quad \text{Eq. 1}$$

where C is the concentration of $(NH_4)_2Fe(SO_4)_2 \cdot 6H_2O$ solution. V_0 and V_1 are the volumes of the consumed $(NH_4)_2Fe(SO_4)_2 \cdot 6H_2O$ solution in blank experiment and water sample determination. V_2 is the volume of the water samples (10 mL). f is the dilution time (10 times).

Text S4

The Eq. of the floc indexes

$$FI = \frac{\sum_{i=1}^{N}(Ratio_i \cdot time_i)}{\sum_{i=1}^{N} time_i} \quad \text{Eq. 2}$$

$$S_f(\%) = \frac{FI_1}{FI_0} \times 100 \quad \text{Eq. 3}$$

$$R_f(\%) = \frac{FI_2 - FI_1}{FI_0 - FI_1} * 100 \quad \text{Eq. 4}$$

where FI_0, FI_1 and FI_2 are the FI values in the steady phase, breakage phase and re-steady phase, respectively. $Ratio_i$ is a certain Ratio value, and $time_i$ is the corresponding time to get $Ratio_i$. FI is positively related to the floc size and provides valuable information of the aggregate growth. Big values of S_f indicate that flocs are strong and resistant, while small values of it mean that the flocs are fragile. Big values of R_f show that flocs can regenerate easily after being broken, while flocs

with small R_f values are difficult to recover.

$$TWV = \frac{\sqrt{\sum_{i=1}^{N}[(Ratio_i - \overline{Ratio})^2 \cdot time_i] / \sum_{i=1}^{N} time_i}}{\overline{Ratio}} \times 100 \qquad \text{Eq. 5}$$

where $\overline{Ratio}$ is the average values of all Ratios. A smaller value of TWV indicates the more compact structure of flocs, while larger value of TWV demonstrates that the aggregates are looser, more porous and highly branched.

$$Settelment\ rate\ (s^{-1}) = \frac{|\Delta Ratio|}{|\Delta Time|} \qquad \text{Eq. 6}$$

settlement rate, calculated from the slope in the sedimentation phase, was closely related to the sedimentation performances of flocs.

Text S5

Characteristics of AL and PSBF

1. FTIR analysis

FTIR spectra of AL and PSBF are shown in Fig. S1a. New peaks at 1721 cm^{-1} and 1477 cm^{-1} were appeared in the spectrum of PSBF, which were absent in AL spectrum. The aforementioned two peaks were assigned to the C=O on DMC monomers and the C-H on $-N^{+}(CH_3)_3$ groups (Huang et al., 2017; Liang et al., 2020). The appearance of the two characteristic peaks in PSBF spectrum confirmed the successful introducing of DMC monomers.

2. TGA analysis and TEM image

The TGA curves of the AL and PSBF are shown in Fig. S1b. The thermal behaviors of PSBF were significantly different from those of AL, which further corroborated the successful occurrence of

the graft copolymerization. An insignificant weight loss of AL was displayed with the temperature lower than 725□. The weight loss of 4.61%, 6.55%, 35.58% and 17.18% was sequentially observed in PSBF curve, which was due to the evaporation of the moisture (Shak and Wu, 2017), decomposition of the AL backbone (Agbovi and Wilson, 2018), pyrogenic degradation of the quaternary ammonium groups (Kong et al., 2015) and the occurrence of the char formation (Sanchez-Silva et al., 2012), respectively. Remarkably, the char formation of AL occurred at around 725□, but the copolymerization accelerated the carbonization process. It indicated that the introduction of $-N^{+}(CH_3)_3$ essentially weakened the thermal stability of AL.

The new endothermic peaks of PSBF at around 725□, 320□, 430□ and 540□ inherently illustrated the successful graft copolymerization (Fig. S1c). Hydrogen bonds were destructed after the introduction of the $-N^{+}(CH_3)_3$. The weakened intermolecular bonding energies coupling with the enhanced charge densities increased the distance in flocculant molecules, leading to the formation of loose polymers (Agbovi and Wilson, 2018). The loose and branched architectures of PSBF accelerated its thermal decomposition (Liu et al., 2017). The conclusions were in line with the result of the TEM image, which exhibited that the PSBF had branched structures with abundant side chains (Fig. S1d).

3. XRD analysis

XRD patterns in Fig. S1e exhibited that some dispersion peaks at 31.9°, 45.7°, 56.5°, 75.4°were observed in AL spectrum but absent in PSBF spectrum. It demonstrated that a loss in the crystallinity occurred after modification owing to the damage of the inherent structure of AL (Tupa et al., 2015). The destruction in the crystallization illustrated that the graft copolymerization was occurred in the crystal region of the AL.

4. Zeta-pH profiles and molecular weight distribution

PSBF was designed as a positively charged macropolymer, the charge density of 1.0 g/L PSBF solution was 4.56×10^{-3} eq/L. The zeta-pH profiles of PSBF, PAC, and PAM are exhibited in Fig. S1f. AL showed electronegativity at pH 2.0-11.0 as our previous study reported (Guo et al., 2019). The successful modification of AL significantly changed its surface charge properties, PSBF exhibited highly cationic properties in the whole measured pH levels. Also, the charge properties of PSBF were more insensitive to pH changing than those of commercial PAC and PAM. The zeta potentials of PAC and PAM turned to be negative as pH attained 10.0. PAC was highly dependent on the pH conditions, which showed cationic properties only at pH level of 5.0-9.0.

Fig. S1g shows the molecular weight distribution of PSBF. The average molecular weight of PSBF was 3.099×10^{5} g/mol, which was lower than that of commercial PAM (10^{6} g/mol). Although the molecular weight of PSBF was relatively low, its charge properties were more excellent than PAM and even PAC. The coagulation-flocculation efficiencies were simultaneously decided by the charge properties and molecular weights, which were investigated in the next sections.

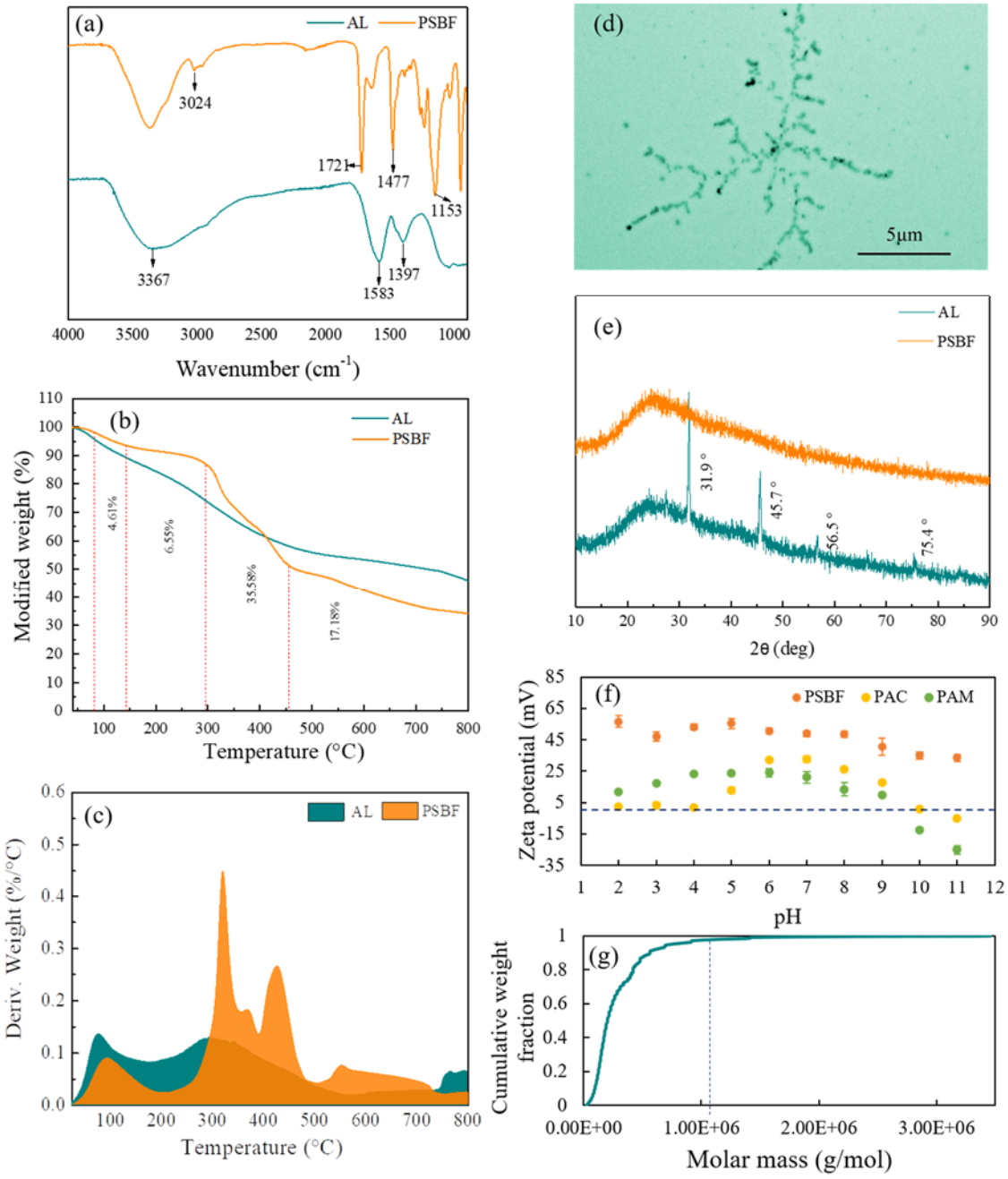

Fig. S1 FTIR spectra (a), TGA curves (b-c), TEM image (d), XRD patterns (e) of AL or PSBF, zeta-pH profiles of the flocculants (f) and molecular weight distribution of PSBF (g).

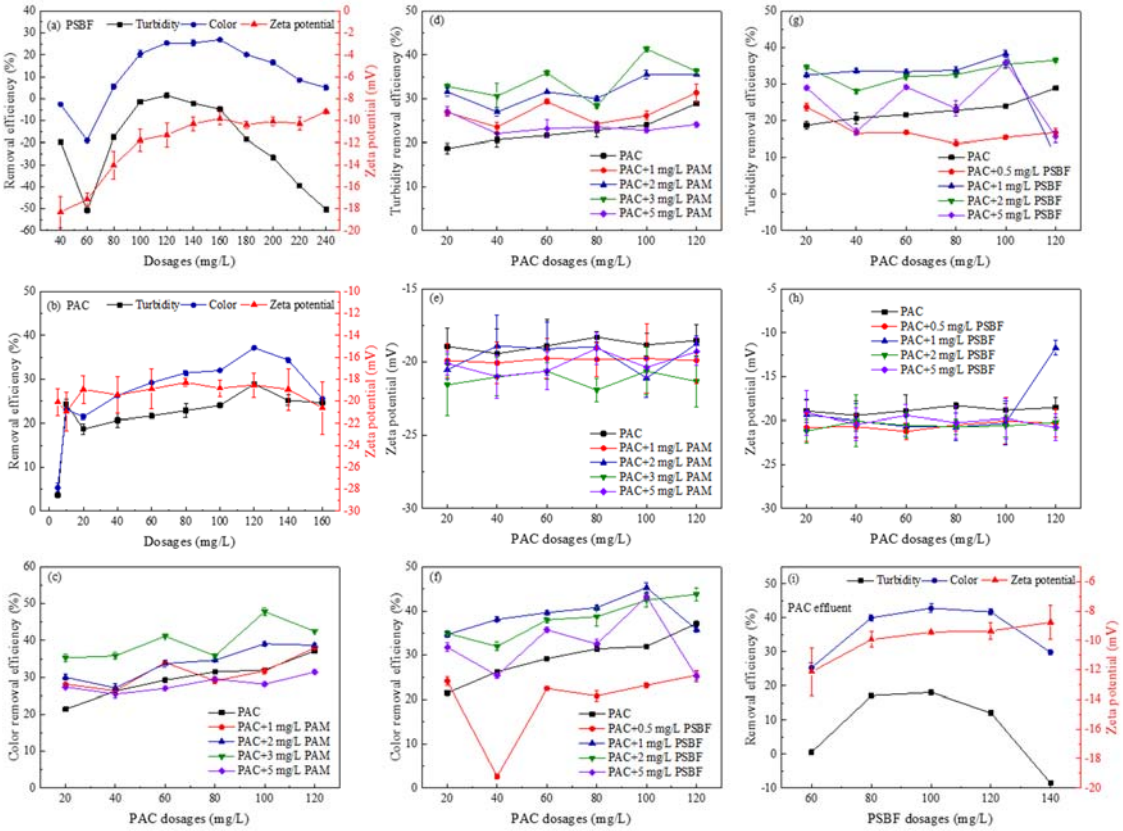

Fig. S2 The color removals, turbidity removals and zeta potentials of flocs with the increasing dosages of different coagulants/flocculants.

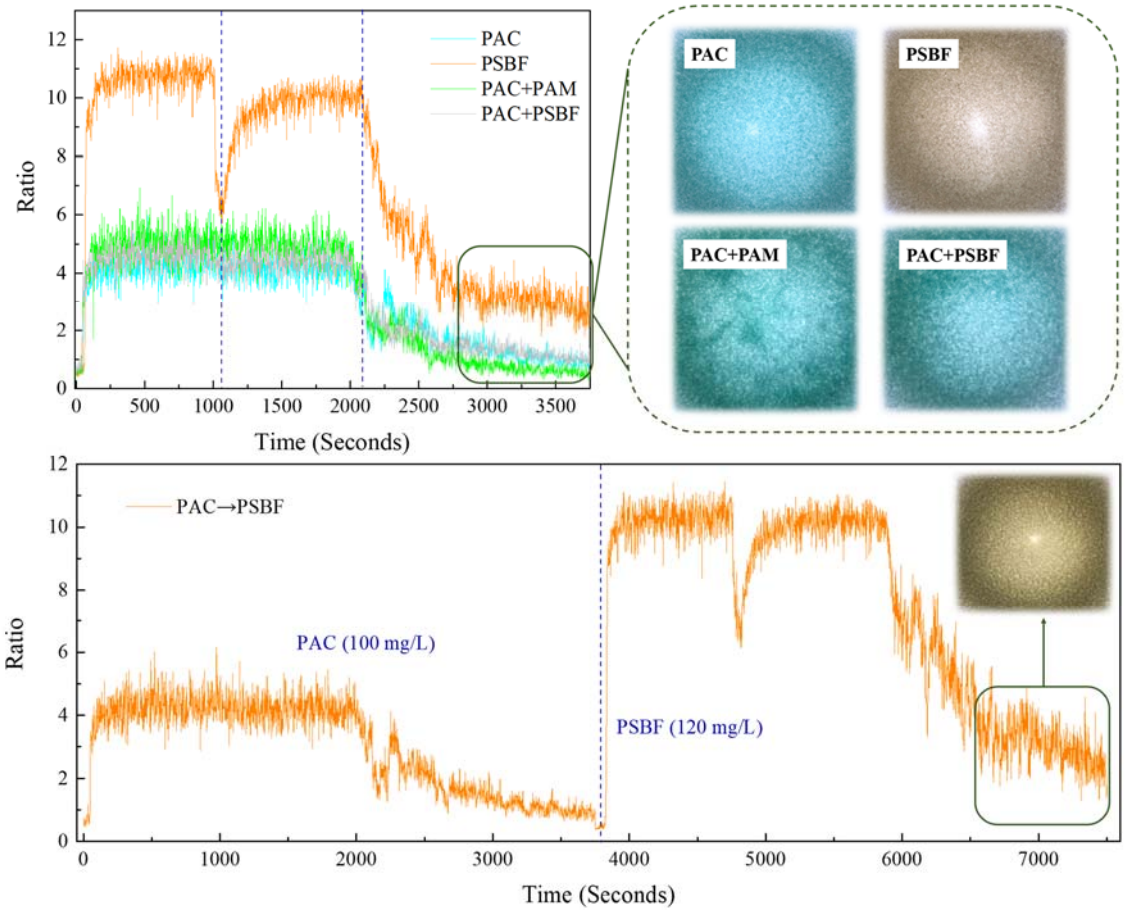

Fig. S3 The growth curves and the pictures of flocs under different coagulation-flocculation systems. The dosages of PAC and PAM were 100 mg/L (in aluminium) and 3 mg/L. The dosage of PSBF was 1 mg/L in PAC+PSBF systems and 120 mg/L in PSBF or PAC→PSBF system. The pH of PPDW was 12.40 ± 0.15.

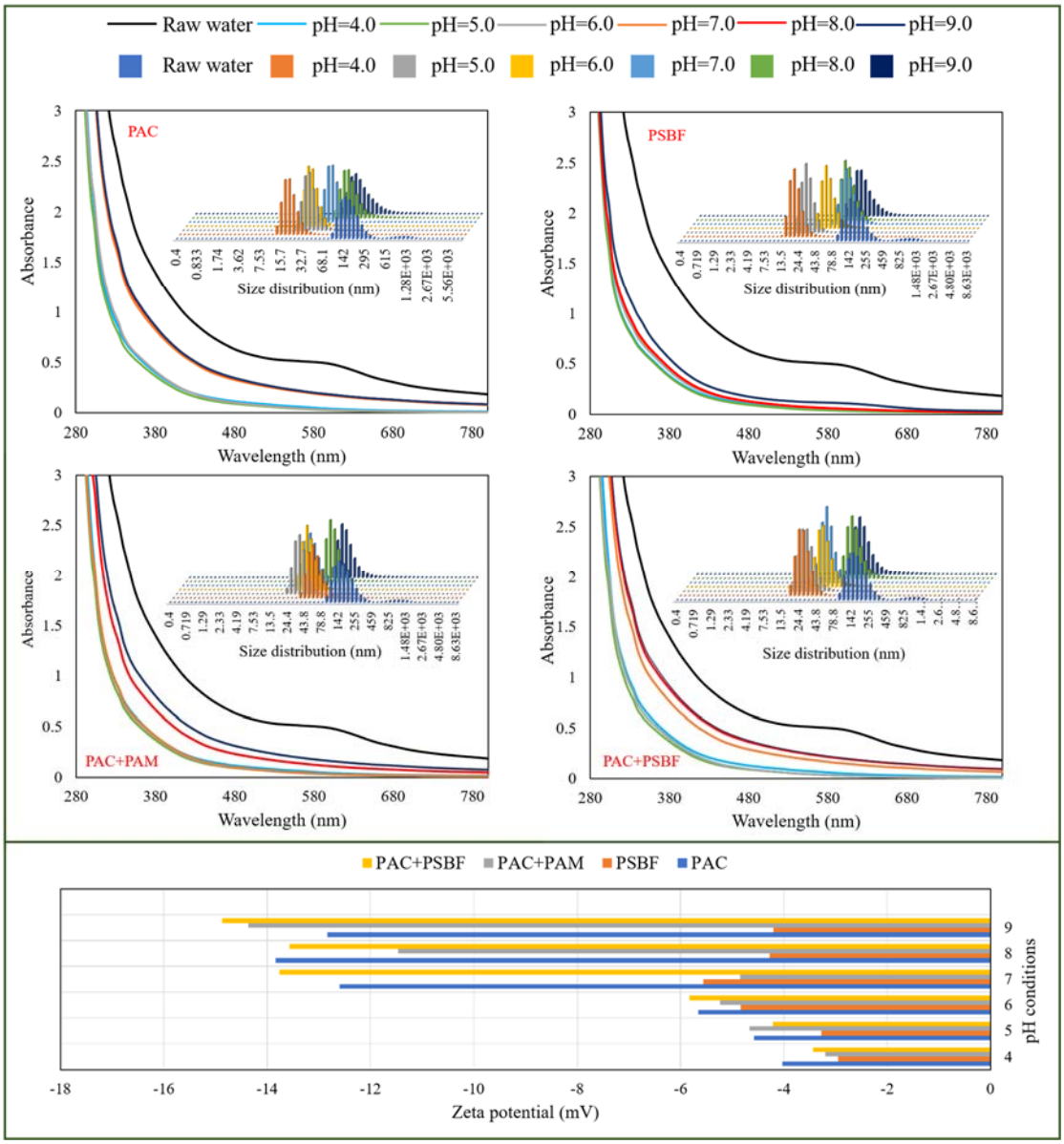

Fig. S4 UV-visible spectrum results of the effluents and the size distributions of residual pollutants (a-d), as well as zeta potentials of flocs (e) in different coagulation-flocculation systems under various pH conditions. The dosages of PAC and PAM were 100 mg/L (in aluminium) and 3 mg/L. The dosage of PSBF was 1 mg/L in PAC+PSBF systems and 120 mg/L in PSBF system.

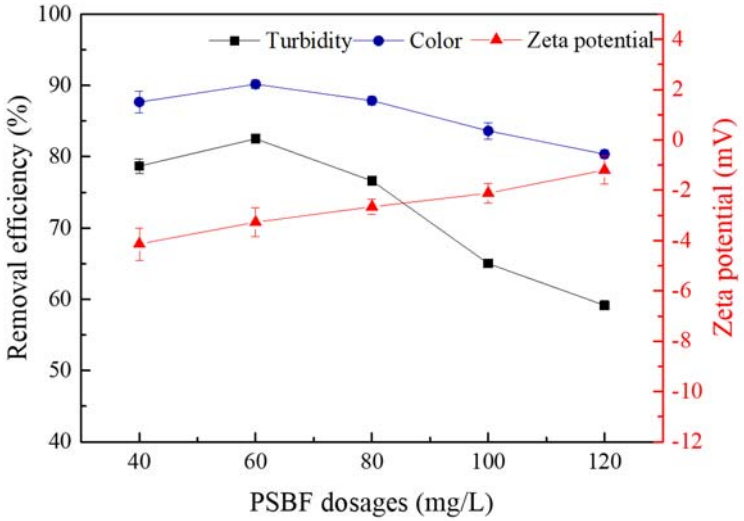

Fig. S5 Turbidity removals, color removals and zeta potentials with the increasing of PSBF dosages in PAC→PSBF system (PAC dosage: 100 mg/L, pH=7.0).

References

Agbovi H K, Wilson L D (2018). Design of amphoteric chitosan flocculants for phosphate and turbidity removal in wastewater. Carbohydrate Polymers, 189: 360-370

Guo K, Gao B, Wang W, Yue Q, Xu X (2019). Evaluation of molecular weight, chain architectures and charge densities of various lignin-based flocculants for dye wastewater treatment. Chemosphere, 215: 214-226

Huang M, Liu Z, Li A, Yang H (2017). Dual functionality of a graft starch flocculant: Flocculation and antibacterial performance. Journal of Environmental Management, 196: 63-71

Kong F, Parhiala K, Wang S, Fatehi P (2015). Preparation of cationic softwood kraft lignin and its application in dye removal. European Polymer Journal, 67: 335-345

Liang S, Zhang T, Fu X, Zhu C, Mou H (2020). Partially degraded chitosan-based flocculation to achieve effective deodorization of oyster (Crassostrea gigas) hydrolysates. Carbohydrate Polymers, 234: 115948

Liu Z, Wei H, Li A, Yang H (2017). Evaluation of structural effects on the flocculation performance of a

co-graft starch-based flocculant. Water Resesrch, 118: 160-166

Sanchez-Silva L, Lopez-Gonzalez D, Villasenor J, Sanchez P, Valverde J L (2012). Thermogravimetric-mass spectrometric analysis of lignocellulosic and marine biomass pyrolysis. Bioresource Technology, 109: 163-172

Shak K P Y, Wu T Y (2017). Synthesis and characterization of a plant-based seed gum via etherification for effective treatment of high-strength agro-industrial wastewater. Chemical Engineering Journal, 307: 928-938

Tupa M V, Avila Ramirez J A, Vazquez A, Foresti M L (2015). Organocatalytic acetylation of starch: effect of reaction conditions on DS and characterisation of esterified granules. Food Chem, 170: 295-302